J Mater Sci: Mater Electron (2016) 27:1244–1253
DOI 10.1007/s10854-015-3882-6

Photo-degradation of organic dyes: simple chemical synthesis of $Ni(OH)_2$ nanoparticles, $Ni/Ni(OH)_2$ and Ni/NiO magnetic nanocomposites

Seyede Raheleh Yousefi[1] · Davood Ghanbari[2] · Masoud Salavati-Niasari[1] · Mohammad Hassanpour[1]

Received: 9 September 2015 / Accepted: 10 October 2015 / Published online: 17 October 2015

Abstract In this work Ni, $Ni(OH)_2$, NiO nanoparticles as well as $Ni/Ni(OH)_2$ and Ni/NiO nanocomposites were synthesized via a simple chemical precipitation method in aqueous solution. The prepared products were characterized by X-ray diffraction pattern (XRD), scanning electron microscopy (SEM), transmission electron microscopy (TEM) and Fourier transform infrared (FT-IR) spectroscopy. Alternating gradient force magnetometer (AGFM) illustrated ferro-magnetic behaviour of Ni nanoparticles as well as $Ni/Ni(OH)_2$ and Ni/NiO nanocomposites. The photocatalytic behaviour of Ni–NiO nanocomposites was evaluated using the degradation of organic dyes under ultraviolet light irradiation. The results show that Ni–NiO nanocomposites have applicable magnetic and photocatalytic performance.

1 Introduction

Magnetic metal–metal oxide core–shell nanoparticles have been the object of a vast amount of material research studies in the last years, because of their phenomenal applications in industry like catalyst, magnetic recording and nano-medicine [1]. This effect can be tuneable through control of core/shell structure, metal/oxide interface quality, shell thickness and oxide composition. Therefore, the possibility to achieve an accurate control is a fundamental step for the optimization of the desired magnetic properties. Ni/NiO systems are of major interest because the high Néel temperature value of NiO ($T_N = 525$ K). The Ni core maintained its metallic nature even after prolonged exposure to atmospheric condition [2]. NiO has been regarded as one of the most promising candidates to replace the commercial graphite anode for lithium-ion batteries, owing to its relatively high theoretical specific capacity (718 mAh g^{-1}), low cost, eco-friendliness and abundance on earth [3]. NiO has a higher density (6.8 g cm^{-3}) than graphite (2.2 g cm^{-3}), which enables simple machining technology. However, the poor electrical conductivity and large volume swing during cycling hinder the practical application of NiO anode [3, 4]. Carbon has been most commonly used to form composite with NiO to reinforce the conductivity and buffer the volume change during the charge/discharge process. Bulk nickel oxide possesses antiferromagnetic characteristic [5–8]. Its magnetic properties are very sensitive on the particle size and broad spectrum of magnetic properties has been obtained in the nanosized systems such as super para-magnetism, spin glass, high magnetization, and high magnetic moment of the particles, high coercivity, high exchange bias, memory and aging effects [9]. Therefore, NiO magnetic properties arise from both the atoms which reside on the surface of the nanoparticles, and from the atoms in the nanoparticle crystalline core. NiO is one of the most exhaustively investigated transition metal oxide due to its high electrochromic efficiency, large modulation range, good cyclic reversibility and low material cost that make them promising candidates in several applications. The applications consist of gas storage, heterogeneous catalysis, selective guest adsorption, and sensor technology [10].

The growing demand for eliminating pollutants from water in order to provide clean water has urged innovating

✉ Masoud Salavati-Niasari
Salavati@kashanu.ac.ir

[1] Institute of Nano Science and Nano Technology, University of Kashan, P.O. Box 87317-51167, Kashan, Islamic Republic of Iran

[2] Young Researchers and Elite Club, Arak Branch, Islamic Azad University, Arak, Islamic Republic of Iran

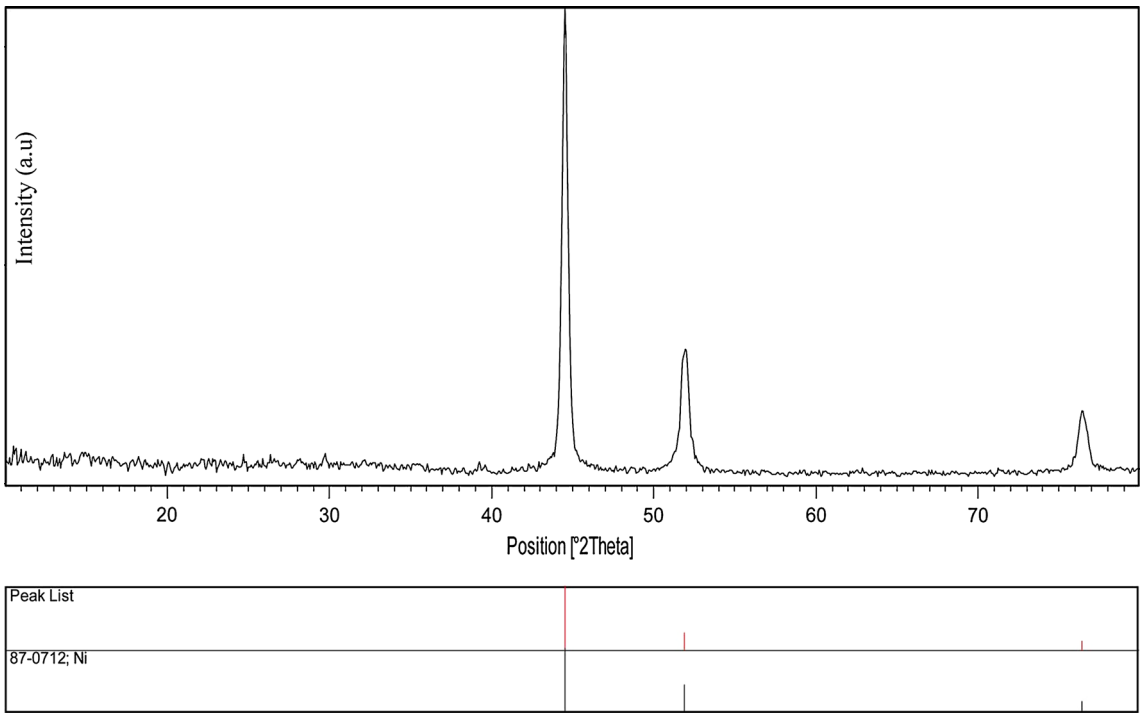

Fig. 1 XRD pattern of nickel nanoparticles

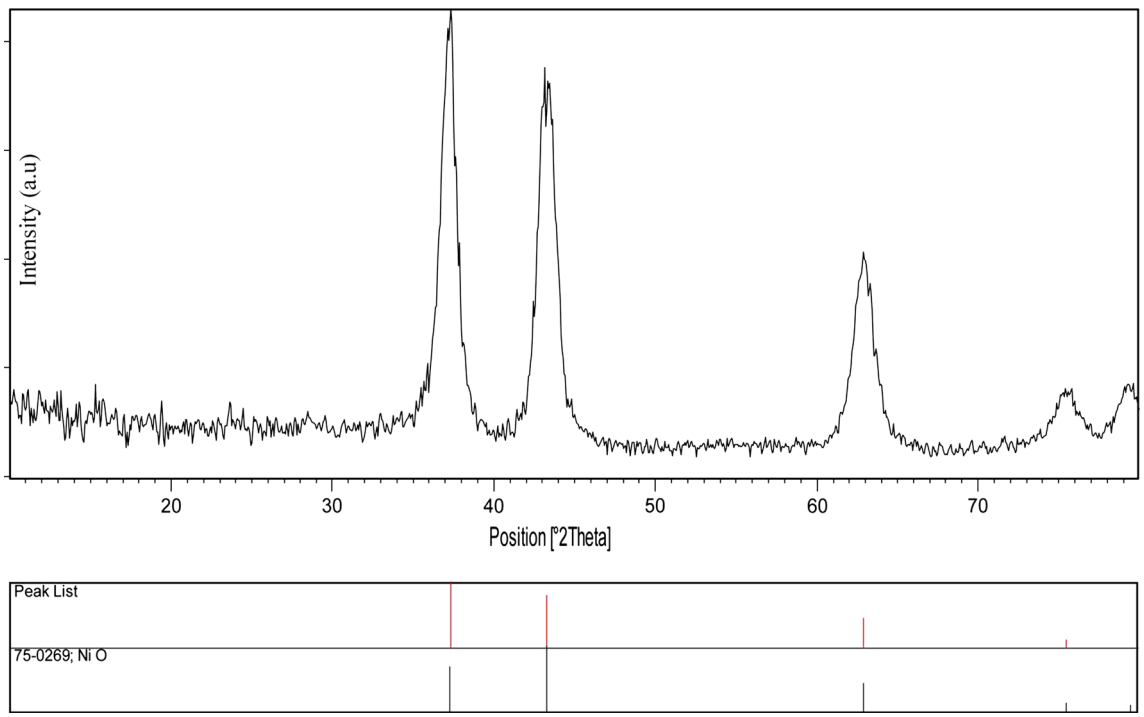

Fig. 2 XRD pattern of NiO nanoparticles

various purification methods and among them, the advanced oxidation processes in which the photo-degradation reactions are included are of great importance. In these processes, organic molecules mainly undergo decomposition reaction by interacting with UV or visible light and a photo-catalyst material to give CO_2 and H_2O as final products [11–15]. NiO nanoparticles exhibit photo-catalytic activity for the decomposition of organic

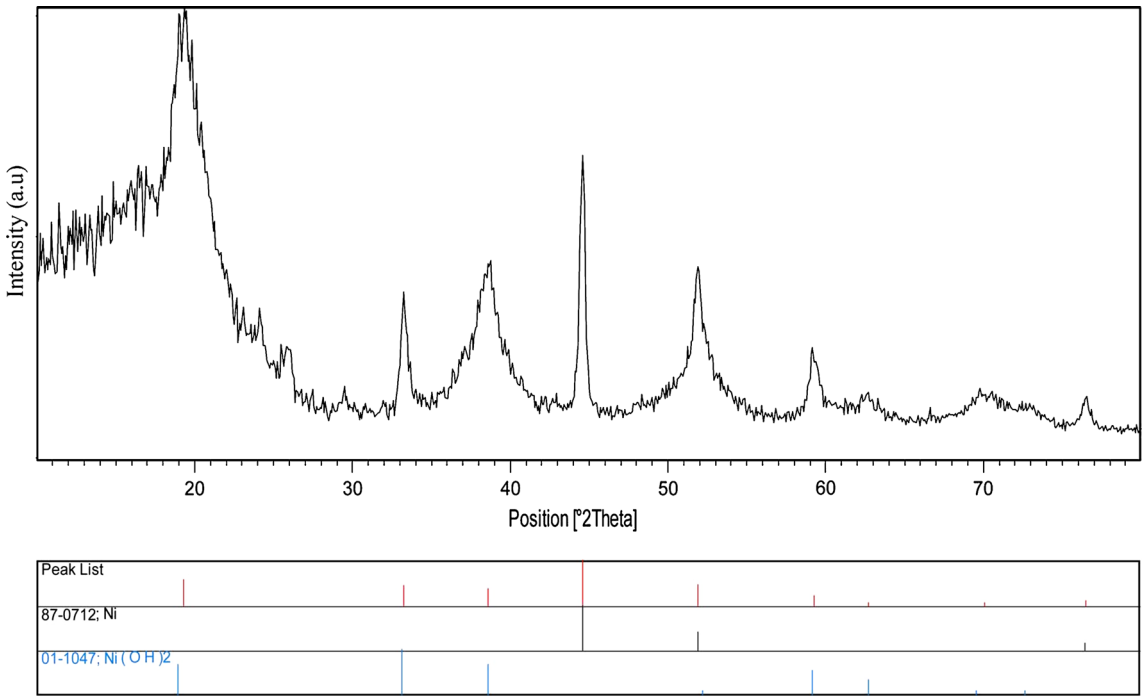

Fig. 3 XRD pattern of $Ni/Ni(OH)_2$ nanocomposite

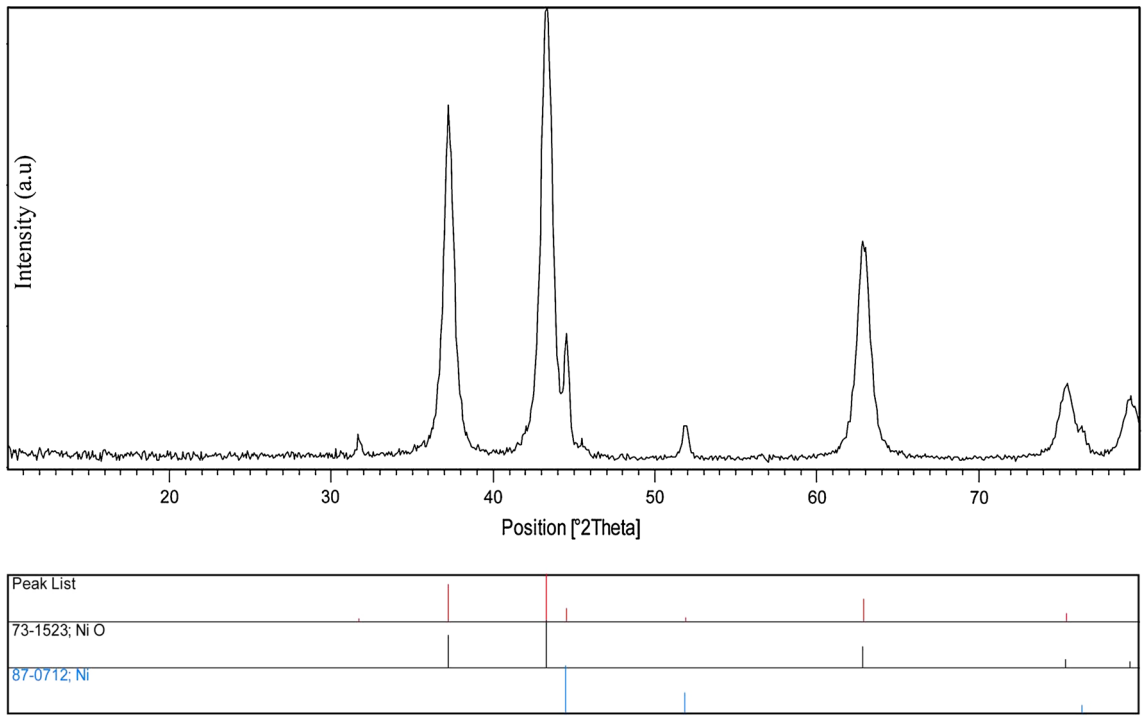

Fig. 4 XRD pattern of Ni/NiO nanocomposite

contaminants. The special properties of magnetic nanoparticles including excellent chemical stability, suitable mechanical hardness, cost-effectiveness and possibility for precise control on the composition along with its ability to be separated by a magnet, has made it a very attractive candidate to be used in nanocomposite photocatalysts [16–20]. Single semiconductor have some problems including high recombination rate of electronic-hole

pairs, low harvest of visible light, poor selective adsorption, photocatalyst deactivation, and high cost of photocatalyst. In order to improve the photocatalytic activity of semiconductor and exploit its advantageous properties, magnetic metal/semiconductor composites have been designed and developed [21–30].

In addition to the possibility for precise control on the composition and structure of nickel and its nanocomposites, a variety of facile chemical and physical synthesis methods have been developed for simple preparation of nickel and nickel hydroxide [1–10]. Chemical precipitation approach is a fast and facile way for production of magnetic powders with different morphologies and fine nanoparticles. Obtaining ultrafine materials with desirable properties in a short period of time is the most significant advantages of precipitation method.

In the present work, Ni, $Ni(OH)_2$ as well as NiO nanoparticles and Ni–$Ni(OH)_2$, Ni–NiO nanocomposites were synthesized by a precipitation method. The effect of various precursors was investigated in order to optimize the reaction condition for obtaining an efficient photocatalyst.

2 Experimental

2.1 Materials and methods

Hydrazine hydrate, $Ni(NO_3)_2$ $6H_2O$, $NiCl_2$ $4H_2O$, $NiSO_4$ and cethyl tri methyl ammonium bromide (CTAB) and poly ethylene glycol (PEG:MW 6000) were purchased from Merck and all the chemicals were used as received without further purifications. Room temperature magnetic properties were investigated using an alternating gradient force magnetometer (AGFM) device, (made by Meghnatis Daghigh Kavir Company, Iran) in an applied magnetic field sweeping between ±10,000 Oe. XRD patterns were recorded by a Philips, X-ray diffractometer using Ni-filtered CuK_α radiation. SEM images were obtained using a LEO instrument model 1455 VP. Prior to taking images, the samples were coated by a very thin layer of Pt (using a BAL-TEC SCD 005 sputter coater) to make the sample surface conductor and prevent charge accumulation, and obtaining a better contrast. A multiwave ultrasonic generator (Bandeline MS 73), equipped with a converter/transducer and titanium oscillator,

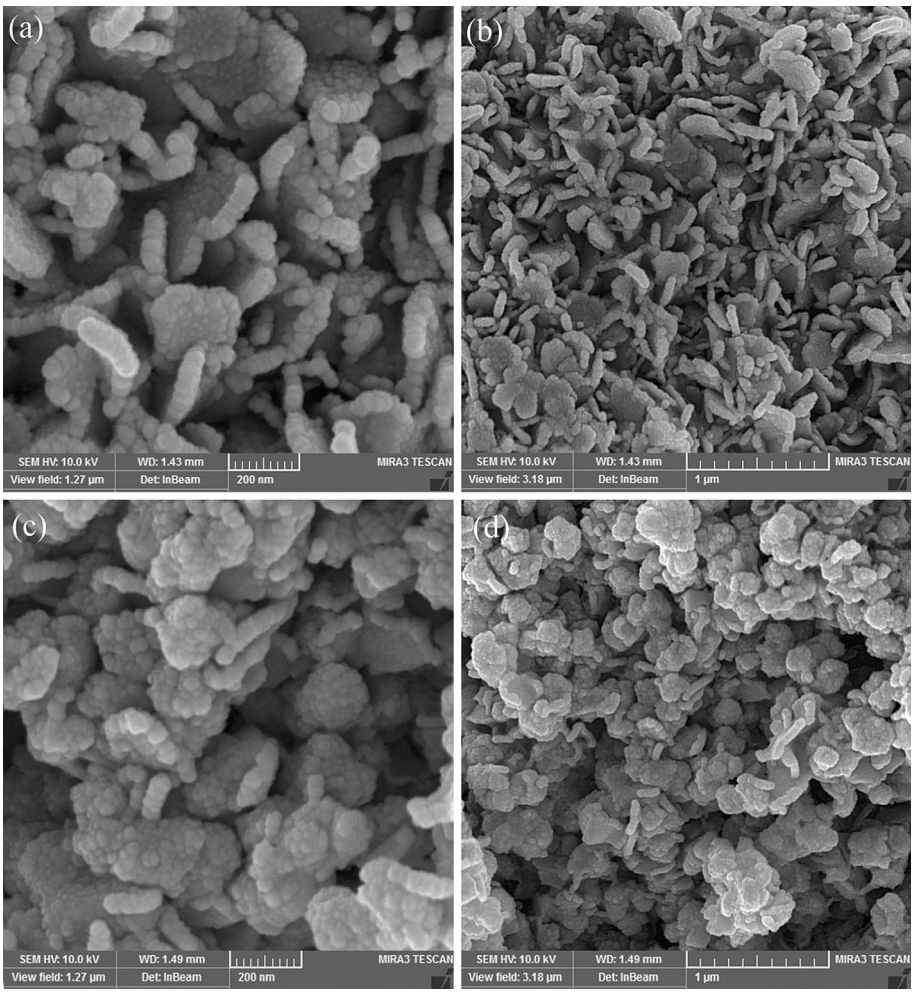

Fig. 5 SEM images of $Ni(OH)_2$ nanoparticles by **a**, **b** PEG; **c**, **d** CTAB

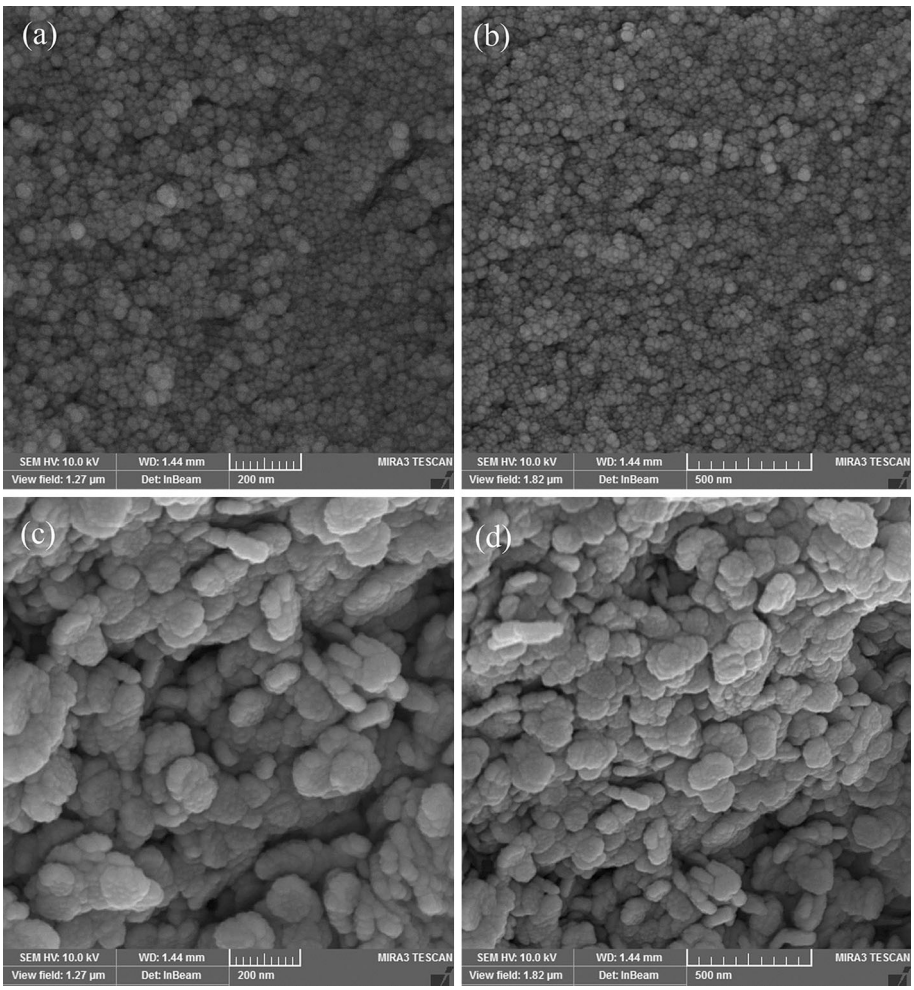

Fig. 6 SEM images of nanoparticles obtained by **a**, **b** nickel sulfate; **c**, **d** nickel chloride

operating at 20 kHz with a maximum power output of 150 W was used for the ultrasonic irradiation.

2.2 Synthesis of nickel nanoparticles

1 g of $NiCl_2$ $4H_2O$ was dissolved in 100 ml of distilled water. 2 ml of hydrazine hydrate solution was slowly added to the solution. Temperature was maintained at 90 °C for 45 min. A black precipitate was obtained confirming the synthesis of nickel. The precipitate of Ni was then centrifuged and rinsed with distilled water. Finally the obtained black precipitate was left to dry at 50 °C.

2.3 Synthesis of $Ni(OH)_2$ and NiO nanoparticles

1 g of $Ni(NO_3)_2$ $6H_2O$ and 0.25 of surfactants (PEG or CTAB) were dissolved in 100 ml of distilled water. 5 ml of ammonia solution was slowly added to the solution. A green precipitate was obtained confirming the synthesis of $Ni(OH)_2$. For preparation of NiO, nickel hydroxide was calcined at 400 °C for 2 h. Finally the obtained black precipitate was left to dry at 50 °C.

2.4 Synthesis of Ni–$Ni(OH)_2$ and Ni–NiO nanocomposites

1 g of nickel nanoparticles were dispersed in water solution and 0.2 g of $Ni(NO_3)_2$ $6H_2O$ was dissolved in the solution simultaneously. 2 ml of ammonia (1 M) was added to solution under ultrasonic irradiation for suitable dispersion. The precipitate of Ni–$Ni(OH)_2$ is then centrifuged and rinsed with distilled water.

3 Results and discussion

Figure 1 shows XRD pattern of nickel Nanoparticles. The XRD pattern of Ni reveals the typical diffraction pattern of pure cubic lattice (JCPDS No.: 87-0712) with Fm-3 m space group which is consistent with previous reports.

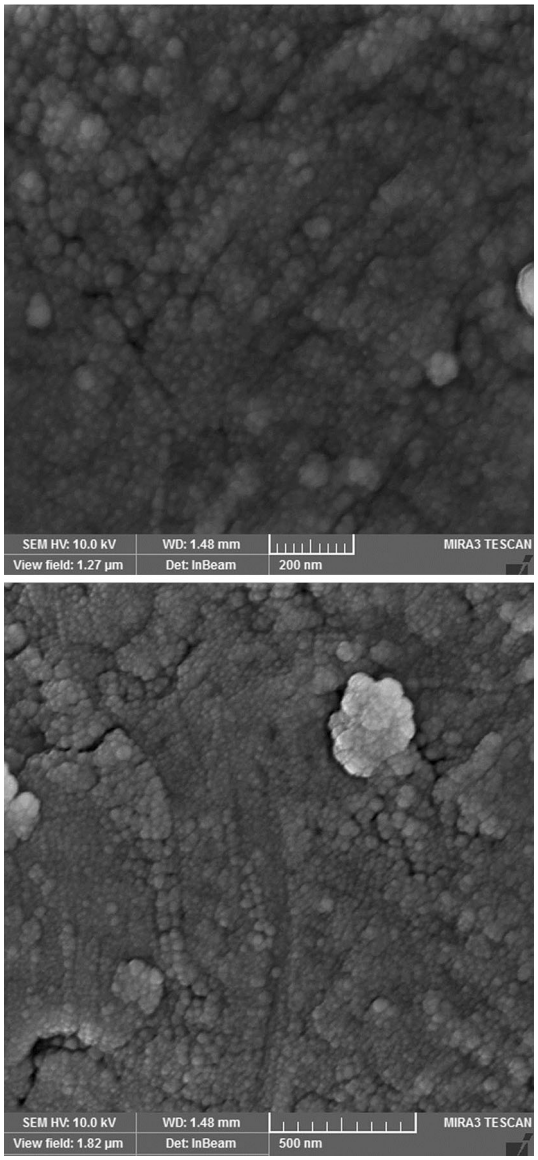

Fig. 7 SEM images of nickel nanoparticles

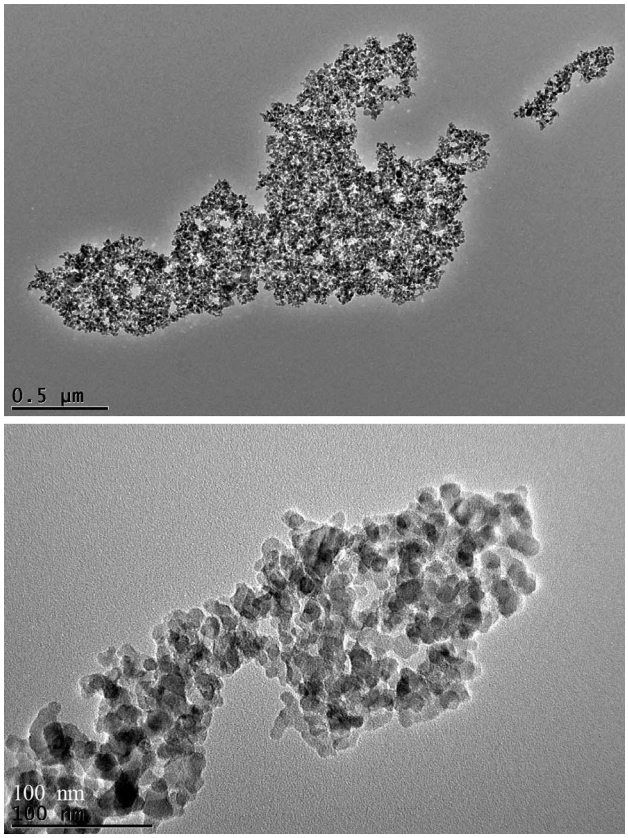

Fig. 8 TEM images of nickel nanoparticles

Figure 2 illustrates XRD pattern including nickel oxide nanoparticles. NiO reveals the typical diffraction pattern of cubic lattice (JCPDS No.: 75-0269) with space group of Fm-3 m. Figure 3 shows XRD pattern of Ni/Ni(OH)$_2$ nanocomposite. It can be observed that both cubic phase of Ni (JCPDS No.: 87-0712, Fm-3 m) and hexagonal phase of Ni(OH)$_2$ (JCPDS No.: 01-1047, space group: *P*-3 m1) are present in the pattern. The structure and composition of the Ni/NiO nanocomposites is also investigated in Fig. 4 by XRD pattern. It also confirms both cubic phase of Ni (JCPDS No.: 87-0712) and cubic phase of NiO (JCPDS No.: 73-1523, Fm-3 m) in the pattern. The intensities of peaks related to each counterpart is relatively similar which is representative of rather equal portion of the shared compounds for in the composite. The calculated crystalline sizes from Scherrer equation, $D_c = K\lambda/\beta Cos\theta$, where β is the width of the observed diffraction peak at its half maximum intensity (FWHM), K is the shape factor, which takes a value of about 0.9, and λ is the X-ray wavelength (CuK_α radiation, equals to 0.154 nm) were about 20 and 14 nm for Ni and NiO nanoparticles, respectively.

Figure 5a, b illustrate SEM images of the as-synthesized Ni(OH)$_2$ nanoparticles obtained by polyethylene glycol, according to electronic microscopy images worm-like nanostructures with average diameter size less than 50 nm were prepared and the crystal growth is faster than nucleation.

Figure 5c, d illustrate SEM images of the another worm-like product obtained by cethyl tri methyl ammonium bromide, that confirms worm-like nanoparticles with mediocre size about 60 nm were synthesized.

Figure 6a, b exhibit SEM images of Ni(OH)$_2$ that achieved by nickel sulfate, images approve particle size between 10 and 20 nm. Figure 6c, d show SEM images of product that achieved by nickel chloride, it is observed that by changing precursor morphology totally was changed, the agglomeration size increase to 10–40 nm. The balance between nucleation rate and growth rate which determines final particle size and morphology depends on precursors and surfactants.

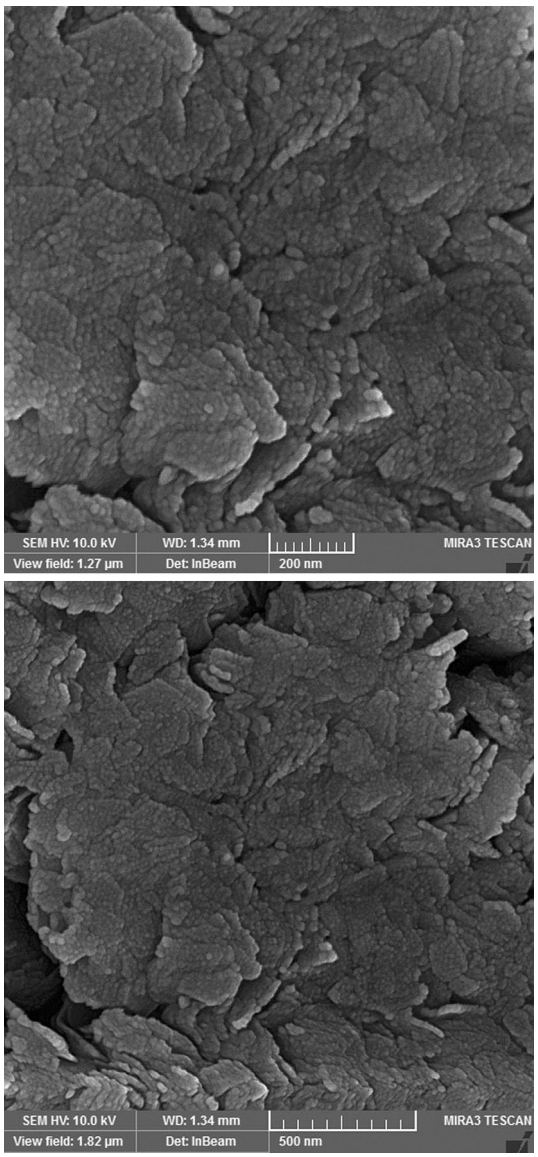

Fig. 9 SEM images of Ni–NiO nanocomposite

Figure 7a, b show SEM images of the prepared magnetic nickel and show mediocre size of nanoparticles are <100 nm. For better estimation of particle size transmission electron microscopy was used, TEM image of Ni nanoparticles are shown in Fig. 8 and confirm nanoparticles with average particle size about 15 nm. Figure 9a, b exhibit SEM images of Ni–NiO nanocomposite that were prepared for photo-catalytic tests, images approve size between 20 and 50 nm.

Figure 10a, b shows the FT-IR spectra of the as-prepared $Ni(OH)_2$ nanoparticles prepared by CTAB and PEG respectively. The absorption bands at 458 and 526 cm^{-1} are assigned to the Ni–O (metal–oxygen) stretching mode.

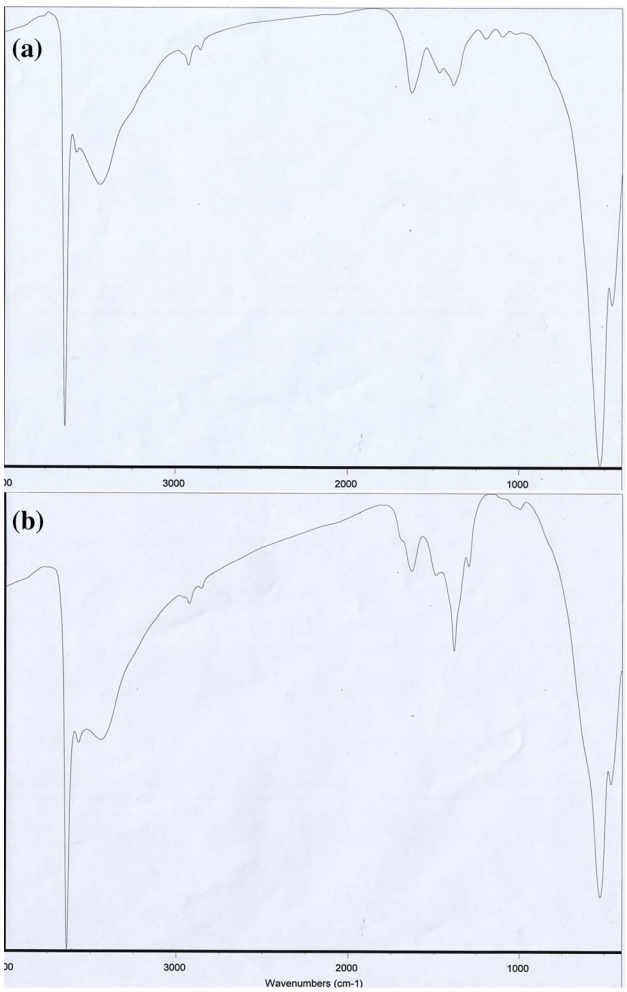

Fig. 10 FT-IR spectra of $Ni(OH)_2$ obtained by **a** CTAB, **b** PEG

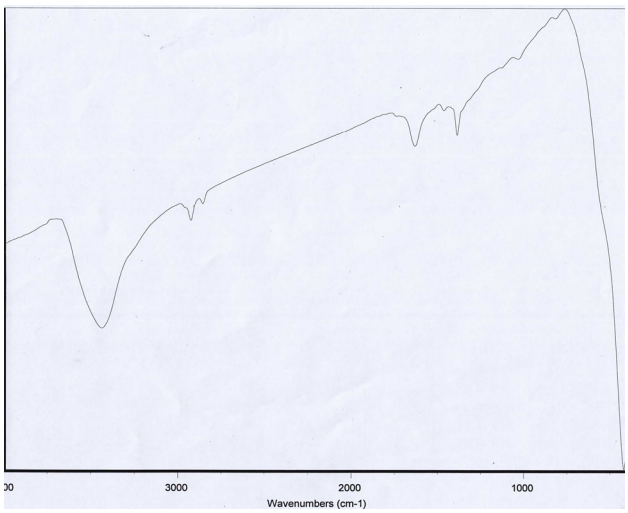

Fig. 11 FT-IR spectrum of NiO nanoparticles

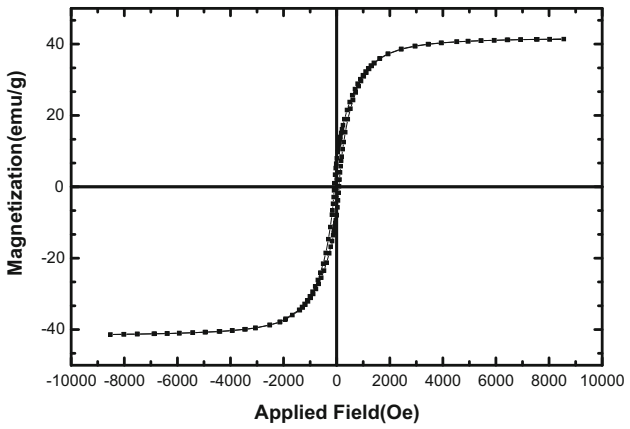

Fig. 12 Room temperature hysteresis loop of Ni nanoparticles

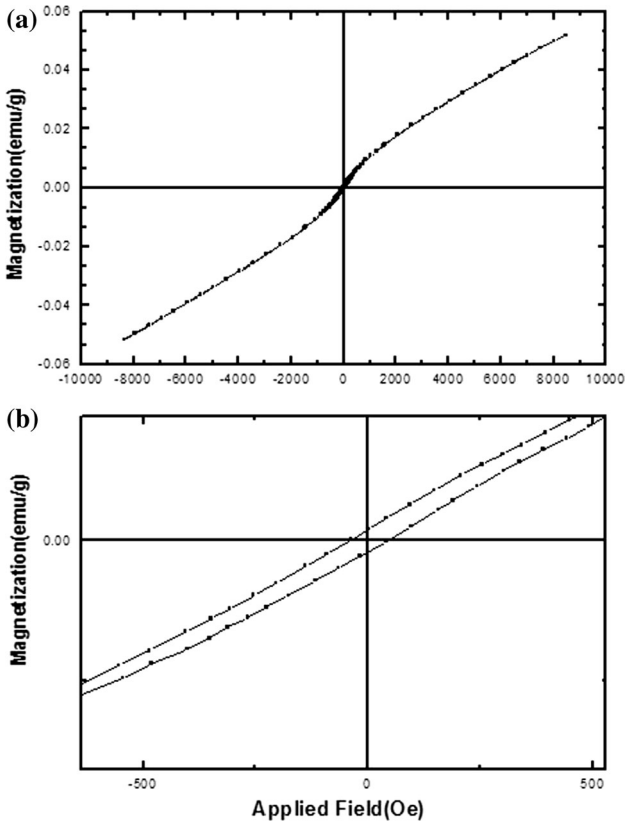

Fig. 13 Hysteresis curves of NiO nanoparticles

The spectrum exhibits broad absorption peaks between 3400 and 3500 cm^{-1}, corresponding to the stretching mode of O–H group of adsorbed hydroxyl group while absorption at 3637 is related to O–H group of nickel hydroxide and the weak band near 1620 cm^{-1} is assigned to H–O–H bending vibration mode due to the adsorption of moisture on the surface of nanoparticles Fig. 11 shows the FT-IR spectra of the as-prepared NiO nanoparticles. It can be observed that the strong absorption band at 418 cm^{-1} which is ascribed

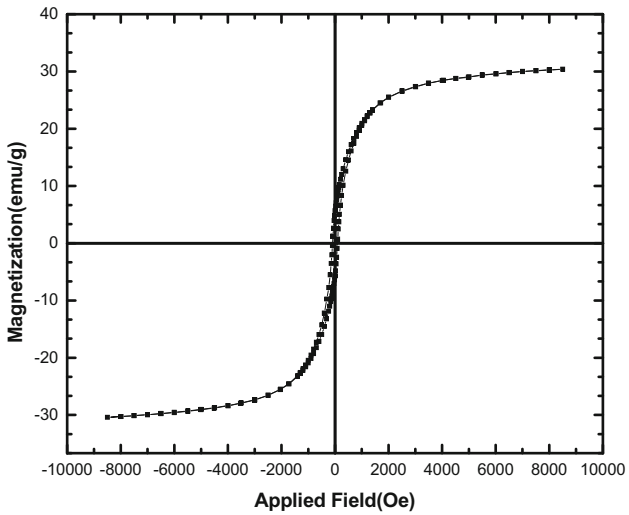

Fig. 14 Hysteresis loop of Ni–$Ni(OH)_2$ nanocomposite

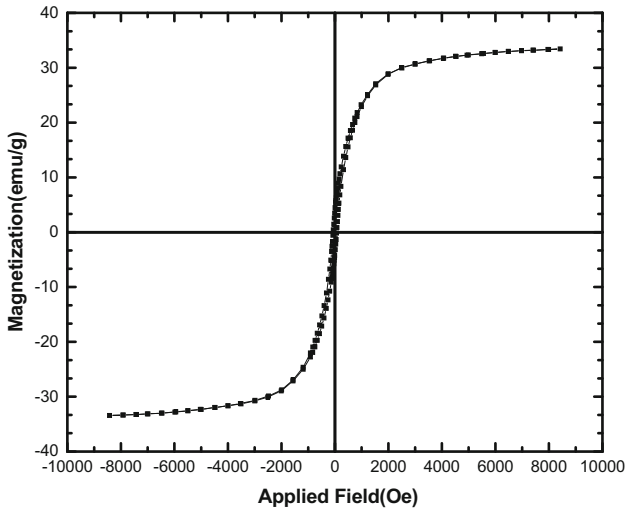

Fig. 15 Hysteresis loop of Ni–NiO nanocomposite

to phonon absorptions of the NiO lattice and broad absorption peaks between 3400 and 3500 cm^{-1} is related to adsorbed O–H groups on the surface of nanoparticles. There are no other significant peaks related to precursors and other impurities.

Room temperature magnetic properties of samples were studied using AGFM device. Hysteresis loop for magnetic nickel nanoparticles is shown in Fig. 12. This shows a sufficient magnetization of these Ni nanoparticles for being recycled by a magnet, making them appropriate for core of recyclable photocatalyst. As-synthesized nickel nanoparticles show ferromagnetic behaviour and have a saturation magnetization of 42 emu/g and a coercivity about 87. Figure 13 illustrates magnetization curve of NiO nanoparticles that approves paramagnetic behavior with a coercivity

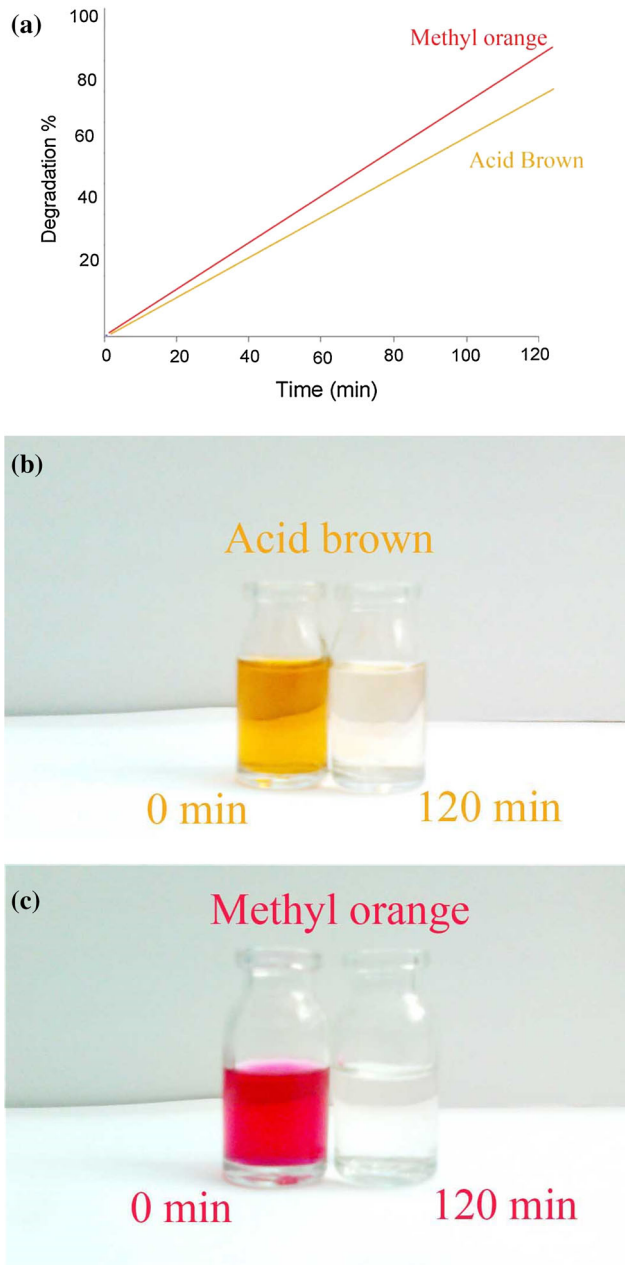

Fig. 16 **a** Photocatalytic activity of Ni/NiO on degradation, **b** acid brown, **c** methyl orange

about 43 and a saturation magnetization of 0.05 emu/g. Figure 14 depicts magnetization curve of Ni–$Ni(OH)_2$ nanocomposites that exhibits ferromagnetic manner with a coercivity around 92 and a saturation magnetization of 30 emu/g. Figure 15 shows magnetization curve of Ni–NiO nanocomposites that also exhibits ferromagnetic behavior with a coercivity about 85 and a saturation magnetization of 33 emu/g. This magnetization indicates that Ni–NiO nanocomposites inherit the magnetic property from the Ni NPs; however, the magnetization is lower due to presence of nickel hydroxide and nickel oxide. This reduction in saturation magnetization is due to the interfacial effect of the typical core–shell nanostructures. The ferromagnetic property of the prepared nanocomposites is an essential characteristic of a regenerable and reusable magnetic heterogeneous catalyst. The results also indicate that Ni–$Ni(OH)_2$ nanocomposite formation give rise to coercivity enhancement. This could be attributed to the addition of $Ni(OH)_2$ on the surface of magnetic nanostructure which changes its magnetic features. A possible explanation for this result could be as follow: The magnetic moments of magnetic nanoparticles are pined by the $Ni(OH)_2$, so that a higher magnetic field is required to align the single domain nanoparticles in the field direction [11, 15].

The photo-catalytic activity of the Ni/NiO nanocomposite was evaluated by monitoring the degradation of organic dyes in an aqueous solution, under irradiation with UV light. The changes in the concentration of dye are illustrated in Fig. 16a. In 120 min methyl orange was degraded about 90 % after 120 min. Acid brown 14 was degraded around 75 % after about 120 min and gave a satisfactory result. Organic dyes decompose to carbon dioxide, water and other less toxic or nontoxic residuals [11, 16]. Figure 16b, c show degradation of the acid brown 14 and methyl orange dyes after 120 min exposure to the Ni–NiO nanocomposite.

4 Conclusions

Firstly, Ni nanoparticles were synthesized via a simple chemical method and the procedure was followed by synthesis of $Ni(OH)_2$ and NiO shell on the surface of the prepared nickel. Effect of PEG, CTAB and various nickel precursor was investigated on morphology and particle size of the products. AGFM confirmed that nanoparticles and nanocomposite exhibit ferromagnetic behaviour. The photocatalytic behaviour of Ni–NiO nanocomposite was evaluated using the degradation of methyl orange and acid brown under UV light irradiation. The results show that chemical method is a suitable method for preparation of Ni-NiO nanocomposites as promising candidate for photocatalytic applications.

References

1. R. Hao, R. Xing, Z. Xu, Y. Hou, S. Gao, S.H. Sun, Adv. Mater. **22**, 2729 (2010)
2. S. D'Addato, V. Grillo, S. Altieri, R. Tondi, S. Valeri, S. Frabboni, J. Phys. Condens. Matter **23**, 175003 (2011)
3. X. Sun, C. Yan, Y. Chen, W. Si, J. Deng, S. Oswald, L. Liu, O.G. Schmidt, Adv. Energy Mater. **4**, 1300912 (2014)
4. J. Ma, J. Yang, L. Jiao, Y. Mao, T. Wang, X. Duan, J. Lian, W. Zheng, CrystEngComm **14**, 453 (2012)

5. Y. Mao, Q. Kong, B. Guo, L. Shen, Z. Wang, L. Chen, Electrochim. Acta **105**, 162 (2013)
6. M.-Y. Cheng, B.-J. Hwang, J. Power Sources **195**, 4977 (2010)
7. X.H. Huang, J.P. Tu, C.Q. Zhang, X.T. Chen, Y.F. Yuan, H.M. Wu, Electrochim. Acta **52**, 4177 (2007)
8. G. Srinivasan, M. Seehra, Phys. Rev. B **29**, 6295 (1984)
9. M.S. Seehra, P. Dutta, H. Shim, A. Manivannan, Solid State Commun. **129**, 721 (2004)
10. A. Tahmasian, A. Morsali, Inorg. Chim. Acta **387**, 327 (2012)
11. J. Saffari, N. Mir, D. Ghanbari, K. Khandan-Barani, A. Hassanabadi, M.R. Hosseini-Tabatabaei (2015, in press). doi:10.1007/s10854-015-3622-y
12. S. Polisetti, P.A. Deshpande, G. Madras, Ind. Eng. Chem. Res. **50**, 12915 (2011)
13. F. Wang, C. Di Valentin, G. Pacchioni, ChemCatChem **4**, 476 (2012)
14. C. Wu, Y.C. Zhang, Q. Huang, Mater. Lett. **119**, 104 (2014)
15. D. Ghanbari, M. Salavati-Niasari, M. Ghasemi-Kooch, J. Ind. Eng. Chem. **20**, 3970 (2014)
16. A. Esmaeili-Bafghi-Karimabad, D. Ghanbari, M. Salavati-Niasari, L. Nejati-Moghadam, S. Gholamrezaei, J. Mater. Sci. Mater. Electron. **26**, 6970 (2015)
17. S. Singh, K.C. Barick, D. Bahadur, J. Mater. Chem. A **1**, 3325 (2013)
18. J. Huang, S. Liu, L. Kuang, Y. Zhao, T. Jiang, S. Liu, X. Xu, J. Environ. Sci. **25**, 2487 (2013)
19. Y.-Q. Li, S.-Y. Fu, Y.-W. Mai, Polymer **47**, 2127 (2006)
20. W.M. Kim, D. Young Ku, I.-K. Lee, Y.W. Seo, B.-K. Cheong, T.S. Lee, I.-H. Kim, K.S. Lee, Thin Solid Films **473**, 315 (2005)
21. N. Mir, M. Salavati-Niasari, F. Davar, Chem. Eng. J. **181–182**, 779 (2012)
22. J. Saffari, H. Shams, D. Ghanbari, A. Esmaeili, J. Clust. Sci. **25**, 1225 (2014)
23. M. Goudarzi, M. Salavati-Niasari, S.M. Hosseinpour-Mashkani, N. Mir, J. Mater. Sci. Mater. Electron. **26**, 5326 (2015)
24. X. Wei, T. Xie, L. Peng, W. Fu, J. Chen, Q. Gao, G. Hong, D. Wang, J. Phys. Chem. C **115**, 8637 (2011)
25. C. Hu, Z. Gao, X. Yang, Chem. Phys. Lett. **429**, 513 (2006)
26. M. Cernea, S.-G. Sandu, C. Galassi, R. Radu, V. Kuncser, J. Alloys Compd. **561**, 121 (2013)
27. H. Momenian, S. Gholamrezaei, M. Salavati-Niasari, B. Pedram, F. Mozaffar, D. Ghanbari, J. Clust. Sci. **24**, 1031 (2013)
28. J. Saffari, D. Ghanbari, N. Mir, K. Khandan-Barani, J. Ind. Eng. Chem. **20**, 4119 (2014)
29. S. Xuan, W. Jiang, X. Gong, Y. Hu, Z. Chen, J. Phys. Chem. C **113**, 553 (2009)
30. W. Wu, J. Changzhong, V.A.L. Roy, Nanoscale **7**, 38 (2015)